



## Phase analysis of biphoton joint spectra by interference between different SPDC sources

INBAR HURVITZ,<sup>1,\*</sup>  ANATOLY SHUKHIN,<sup>2</sup> LEONID VIDRO,<sup>2</sup> HAGAI EISENBERG,<sup>2</sup> AND ADY ARIE<sup>1</sup> 

<sup>1</sup>School of Electrical Engineering, Fleischman Faculty of Engineering, Tel Aviv University, Tel Aviv 69978, Israel

<sup>2</sup>Racah Institute of Physics, Hebrew University of Jerusalem, Jerusalem 91904, Israel

\*inbarhurvitz@mail.tau.ac.il

Received 22 July 2024; revised 9 September 2024; accepted 21 September 2024; published 17 October 2024

In spontaneous parametric down-conversion, the spectral correlations between the signal and the idler are expressed by the joint spectral amplitude (JSA) function. However, in the standard coincidence measurements, the phase information of the JSA is lost, and only the square of the absolute value of the JSA is recorded, thus preventing full characterization of the biphoton state. Here, we present an experimental technique to investigate the interference of biphoton joint spectral amplitudes, unlocking new avenues in quantum photonics research. Our method explores phase-dependent phenomena within entangled biphoton spectra. This is achieved by simultaneously pumping two structured nonlinear photonic crystals and observing their interference, which reveals previously inaccessible effects with direct intensity measurements. We demonstrate the versatility of our technique by analyzing two types of joint spectra: one exhibiting a two-lobe shape and the other a three-lobe shape. Additionally, we reconstruct the joint spectral amplitudes for both scenarios and observe good agreement with theoretical predictions. These results pave the way for developing advanced quantum communication and information processing technologies using biphoton spectra.

© 2024 Optica Publishing Group under the terms of the [Optica Open Access Publishing Agreement](#)

<https://doi.org/10.1364/OPTICAQ.537375>

### 1. INTRODUCTION

The essence of quantum optics and quantum information technologies [1] hinges on the superposition states of single photons and the entangled states of photon pairs. Streamlining the creation and manipulation of these quantum states is crucial for advancing secure quantum communications, quantum computing, and quantum sensors [2]. Using spontaneous parametric down-conversion (SPDC) [3–5] as a promising method for state generation involves tapping into nonlinear optical effects, which have played a vital role in producing high-purity heralded single photons, entangled photon pairs, and squeezed states [6].

Encoding information in the spectral degree of freedom of photons [7–9] is often preferred in the pursuit of establishing long-distance quantum communication links and scalable quantum networks [10,11]. This approach presents various advantages, such as the possibility for high-dimensional quantum information representation (qudits), using a single spatial channel, e.g., in single-mode optical fibers and waveguides. Thus, more information can be encoded on a single photon, improving the security of quantum key distribution protocols [12,13].

The spectrum of photons generated using domain-engineered nonlinear photonic crystals (NLPCs) has been studied over the past decade [14–18]. These works align with our efforts to manipulate and control the spectral properties of the outcome

of the SPDC process. The generated biphoton state is

$$|\psi\rangle = \iint d\omega_s d\omega_i A(\omega_s, \omega_i) a_h^\dagger(\omega_s) a_v^\dagger(\omega_i) |0\rangle, \quad (1)$$

where  $a_h^\dagger(\omega_s)$  and  $a_v^\dagger(\omega_i)$  represent the creation operators into the signal and idler modes, with horizontal and vertical polarizations, respectively.  $A(\omega_s, \omega_i)$  is the joint spectral amplitude (JSA) of the two-photon field describing the amplitude of generating the signal and idler photons, and their correlations at the respective frequencies  $\omega_s$  and  $\omega_i$ . Nevertheless, conventional characterization methods often rely on coincidence measurements which yield the joint spectral intensity (JSI = |JSA|<sup>2</sup>) without accounting for phase information. Thus, it is hard to distinguish between states that differ in phase by using the JSI measurement.

Accurately measuring the JSA of photon pairs is a challenging task because it requires capturing both spectral amplitude and phase information. While a spectrometer can measure the spectral amplitude, determining the spectral phase is more complicated and requires advanced techniques. There are methods that involve self-referencing approaches using optical nonlinear devices [19], but these are not suitable for single photons due to their weak electric fields and introduce significant experimental complexity and long data integration times. Another approach is to interfere the unknown signal pulse with a well-characterized

reference pulse and perform spectrally resolved detection, which necessitates a precisely known and phase-stable reference pulse.

A previous work [20] demonstrated a scheme based on intensity interferometry to measure the JSA of photon pairs produced by SPDC. In this method, one of the down-converted photons is sent directly into a spectrally resolving single-photon detector, while the other heralded photon is combined with a reference pulse in a single-mode fiber beam splitter. This setup requires a motorized stage to set the delay between the two pulses. While effective, this approach is intricate due to the necessity of the reference pulse, which adds complexity to the measurement process.

In another study [21], the authors explore techniques for controlling the spectral properties of biphotons. They present a method for manipulating the JSA of biphotons, enabling a shaping method for biphoton wave packets. Their manipulation effects are confirmed through JSI measurements and Hong–Ou–Mandel (HOM) interference patterns.

A recent study [22] showed that by using spatially resolved single-photon detection, the spatial structure of biphotons generated through SPDC could be inferred. The analysis in that work focused on isolating the amplitude and phase components of the pump and phase-matching contributions to the two-photon states. The authors demonstrated that by applying a phase retrieval algorithm, the free-space propagation of the pump and phase-matching could be observed. This information can then be used to reconstruct the full biphoton wavefunction, providing a deeper understanding of the spatial properties of the generated biphotons.

Here, we propose and demonstrate a novel approach to exploring the interference between two biphoton JSAs, using crystal-based interferometry in domain-engineered  $\text{KTiOPO}_4$  (KTP) NLPCs. This method provides a compact and robust means to uncover the intricate interplay between quantum states, complementing the investigation into NLPC-generated photon spectra and opening avenues for new insights. By conducting experimental validation and analysis, we showcase the adaptability of our method in exploring four JSAs: two JSAs characterized by a two-lobe configuration and the other two JSAs characterized by a three-lobe configuration. We examine cases of different JSAs that yield (almost) identical JSIs. Subsequently, we interfere two JSAs and measure the resulting intensity, which indicates their internal phase structure. Moreover, we show that under specific conditions, the JSA can be reconstructed from only two JSI measurements. We concentrate on the superposition of distinct JSAs with a relative phase, leading to interference between the biphoton states and providing a complementary approach to the spectral shaping techniques explored in [21].

## 2. THEORY

SPDC involves the interaction of three electromagnetic fields within a nonlinear medium. During this process, a photon from one mode (pump) is annihilated, resulting in the creation of two photons in the other two modes (signal and idler). The process complies with the conservation of energy  $\omega_p = \omega_s + \omega_i$  and momentum  $\Delta k'(\omega_s + \omega_i) = k_p(\omega_s + \omega_i) - k_s(\omega_s) - k_i(\omega_i)$ , where  $\omega_p, \omega_s, \omega_i$  are the angular frequencies of the pump, signal, and idler;  $k_p, k_s, k_i$  are the corresponding wavevectors; and  $\Delta k'$  is the wavevector mismatch that can be compensated using a quasi-phase-matching technique. In this technique, a poling period,  $\Lambda$ , is introduced and chosen to satisfy  $\Delta k' = \pm 2\pi m/\Lambda$ , where  $m$  is

the order of quasi-phase-matching. Now we can define

$$\Delta k(\omega_s, \omega_i) = k_p(\omega_s + \omega_i) - k_s(\omega_s) - k_i(\omega_i) \pm \frac{2\pi m}{\Lambda}. \quad (2)$$

In the low-gain regime, characterized by  $\kappa = \omega \chi^{(2)} E_p L / cn < 1$  (where  $\chi^{(2)}$  represents the susceptibility,  $E_p$  denotes the pump field,  $L$  is the crystal length, and  $n$  is the refractive index) [16], the JSA can be expressed as the product of the pump's spectral distribution,  $P(\omega_s + \omega_i)$ , and the phase-matching function (PMF),  $\Phi(\Delta k(\omega_s, \omega_i))$ , depicted as

$$A(\omega_s, \omega_i) = P(\omega_s + \omega_i) \cdot \Phi(\Delta k(\omega_s, \omega_i)). \quad (3)$$

The PMF is a Fourier transform of the crystal's poling function [23], and in general, it can be written as

$$\Phi(\Delta k(\omega_s, \omega_i)) = \chi^{(2)} \int_{-\infty}^{\infty} d(z) e^{i\Delta k(\omega_s, \omega_i)z} dz, \quad (4)$$

where  $d(z)$  is the poling function describing the sign of the susceptibility as a function of the longitudinal coordinate  $z$ . The PMF can be arbitrarily shaped using a simple analytical formula: by taking the Fourier transform of the desired PMF and normalizing it,  $u(z)$ , we can design the nonlinear crystal as follows [23,24]:


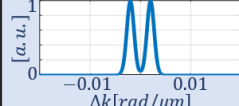


$$d_j(z) = \text{sign} \left[ \cos \left( \frac{2\pi}{\Lambda} z + \varphi_j(z) \right) - \cos(\pi q_j(z)) \right], \quad (5)$$

where  $q_j(z) = \arcsin(|u_j(z)|)/\pi$  and  $\varphi_j$  is the phase of  $u_j(z)$ . This scheme enables to shape the PMF by varying the duty cycle and phase of the (binary) nonlinear modulation. For the case we consider here, of nearly degenerate type II SPDC near 1560 nm, the shaping of the PMF alters the JSA along the anti-diagonal axis. In this work, we used four different crystal designs,  $d_j(z)$ , where  $j = 1, 2, 3, 4$ . Two designs exhibit a two-lobe shape, while the others exhibit a three-lobe shape. Specifics about the NLPCs are provided in Table 1. In this study, we assume plane wave interaction because the length of the NLPCs ( $L = 4$  mm) is much smaller than the confocal parameter of 72 mm.

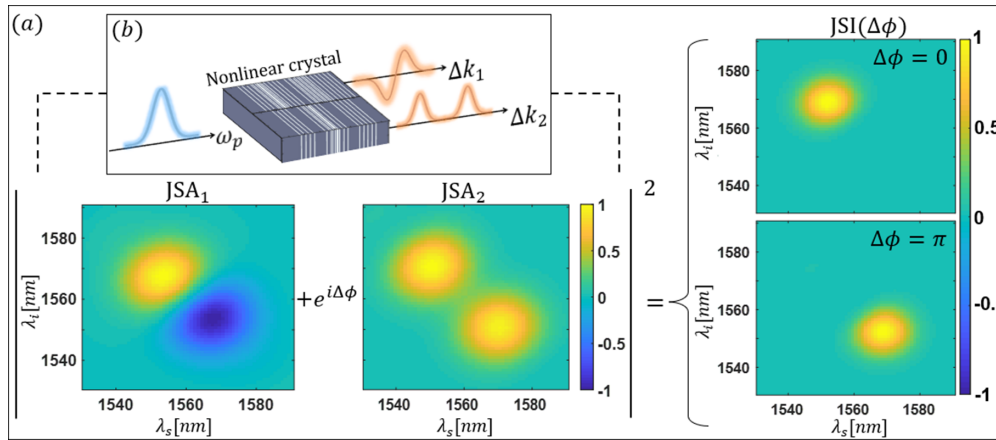
### 2.1. Crystal-Based Interferometry

Our research explores using two NLPCs arranged consecutively or in parallel within the SPDC process. While previous studies have primarily focused on generating polarization entanglement [25–27] or spatial entanglement [28] using this configuration, our work investigates the potential for manipulating and controlling the spectral entanglement of the generated photon pairs. Figure 1 illustrates the principle of crystal-based interferometry. Our research concentrates on investigating the interference phenomenon between two JSAs. Leveraging this interference, we manipulate the JSI while also providing means to differentiate between two JSAs possessing identical JSIs with different phase dependencies through intensity measurements. This approach enables the acquisition of phase information without constructing a standard interferometer, achieved instead by concurrently passing through two domain-engineered NLPCs. Without employing crystal-based interferometry, interfering two SPDC sources typically necessitates constructing a larger and more intricate setup. This conventional approach involves numerous optical elements and an interferometer's precise alignment. The complexity of this setup increases with the need for high stability, making it challenging to maintain over time.

**Table 1.** Detailed table of the Hermite–Gaussian, 2-Gaussian, and 3-Gaussian Designs, Providing  $\Phi(\Delta k(\omega_s, \omega_i))^a$ 

Design	$\Phi(\Delta k(\omega_s, \omega_i))$	
HG <sub>1</sub>	$\frac{(\Delta k)\sqrt{e}}{\sigma_1} e^{-\frac{(\Delta k)^2}{2\sigma_1^2}}$	
2 Gaussians	$\frac{1}{\sqrt{2\pi}\sigma_2} \left( \exp\left(-\frac{(\Delta k - a)^2}{2\sigma_2^2}\right) + \exp\left(-\frac{(\Delta k + a)^2}{2\sigma_2^2}\right) \right)$	
3 Gaussians <sub>1</sub>	$\frac{1}{\sqrt{2\pi}\sigma_3} \left( \exp\left(-\frac{(\Delta k - b)^2}{2\sigma_3^2}\right) + \exp\left(-\frac{(\Delta k)^2}{2\sigma_3^2}\right) - \exp\left(-\frac{(\Delta k + b)^2}{2\sigma_3^2}\right) \right)$	
3 Gaussians <sub>2</sub>	$\frac{1}{\sqrt{2\pi}\sigma_3} \left( -\exp\left(-\frac{(\Delta k - b)^2}{2\sigma_3^2}\right) + \exp\left(-\frac{(\Delta k)^2}{2\sigma_3^2}\right) - \exp\left(-\frac{(\Delta k + b)^2}{2\sigma_3^2}\right) \right)$	

<sup>a</sup>Figures show the phase-matching function versus  $\Delta k$  (which is given in Eq. (4)). For all the crystals, the crystal length is 4 mm, and the poling period is 46  $\mu\text{m}$ . The values of the parameters in the table are:  $\sigma_1 = 2 \times 10^3 [1/\text{m}]$ ,  $\sigma_2 = 1.5 \times 10^3 [1/\text{m}]$ ,  $\sigma_3 = 1 \times 10^3 [1/\text{m}]$ ,  $a = 2 \times 10^3 [1/\text{m}]$ ,  $b = 5 \times 10^3 [1/\text{m}]$ .



**Fig. 1.** Simulation results that show the crystal-based interferometry method. (a) Left-hand side demonstrates the interference of two JSAs ( $\text{JSA}_{1,2}$ ) with a relative phase between them ( $\Delta\phi$ ). Right-hand side depicts the resulting total JSI after the interference for two choices of the relative phase  $\Delta\phi = 0, \pi$ . (b) The two JSAs are created by pumping specialized NLPCs with  $\Delta k_{1,2}$  phase-matching functions. This figure showcases our crystal-based interferometry method and, as an example, the generation of Hermite–Gauss of order 1- (HG<sub>1</sub>) and 2-Gaussian spectra.

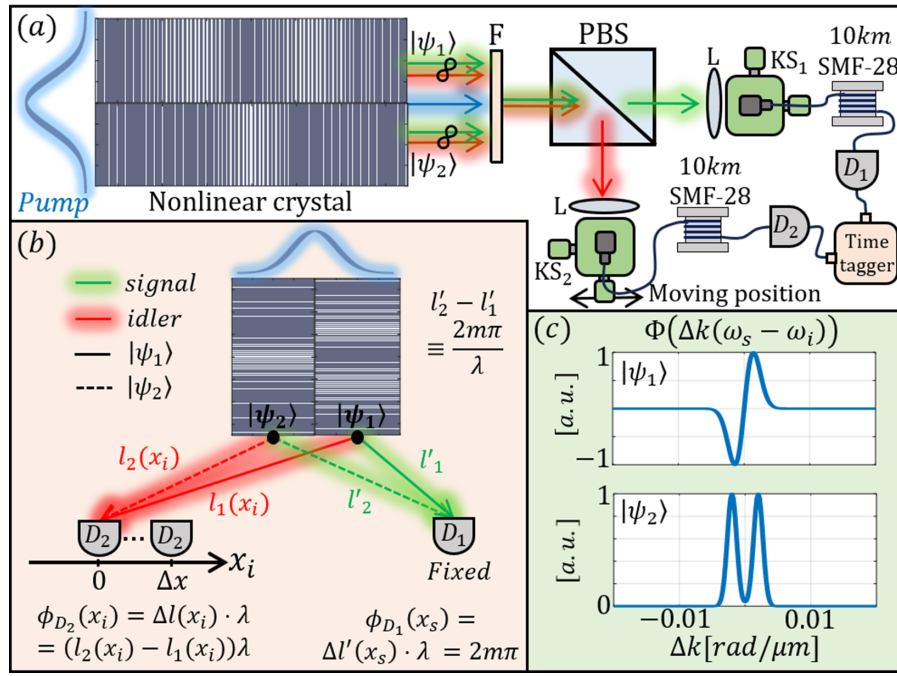
In contrast, crystal-based interferometry simplifies the process by using domain-engineered NLPCs to achieve the interference directly, thereby reducing the need for a complex optical arrangement.

An illustration of the experimental setup for observing SPDC in engineered NLPCs is shown in Fig. 2. The setup includes a tunable pulsed titanium-sapphire (Ti:Sa) laser as the pump source with a pulse duration of 90 fs, a pulse repetition rate of 76 MHz, and a spectral width of approximately 7 nm (FWHM). The central wavelength  $\lambda_{p0}$  was adjusted to 780 nm. The pump is focused into the engineered NLPCs with a waist of approximately 100  $\mu\text{m}$ , where type II SPDC occurs and is then filtered out using a long-pass filter with a cut-off wavelength of 950 nm. Photon pairs generated inside the crystals are split into two arms by a polarizing beam splitter, coupled into single-mode fibers, and detected by superconducting nanowire single-photon detectors (SNSPDs) with a detection efficiency of  $\sim 95\%$  at 1560 nm.

To measure the JSI of generated photons, we applied time-of-flight spectroscopy [29]. Using a 10-km SMF-28 optical fiber in both signal and idler photon arms, we achieved a spectral delay of 180 ps/nm. Comparing correlated photon arrival times with a reference clock allowed us to reconstruct the JSI for different positions of the kinematic stage ( $\text{KS}_2$  in Fig. 2(a)).

The resolution of our time-of-flight measurement setup is primarily determined by the total timing jitter, which includes contributions from the SNSPDs, the time-tagger, and the clock photodiode. Specifically, the timing jitter of the time-tagger (Swabian Ultra) is 140 ps, the SNSPDs (Scontel) have a jitter of 40 ps, and the photodiode used for the clock contributes approximately 35 ps, all expressed as FWHM. By combining the timing jitter values of all components in quadrature, we estimated the overall temporal resolution to be approximately 150 ps.

Crystal-based interferometry has some similarities to the double-slit experiment but uses two detectors for biphoton coincidence measurement, as illustrated in Fig. 2(b). The quantum states ( $|\psi_{1,2}\rangle$ ) are split by polarization, sending the signal



**Fig. 2.** (a) Experimental setup. A Ti:Sa pump pulse passes through a KTP nonlinear crystal, generating a correlated photon pair. The entangled photon pair (signal and idler) undergoes polarization-based splitting, with each routed through a 10-km SMF-28 fiber and detected individually by single-photon detectors. Arrival times are measured using a time tagger. Key components: F, filter; PBS, polarizing beam splitter; KS, fiber coupling kinematic stage; L, lens; D, detector. (b) Illustration of crystal-based interferometry. This method is similar to the double-slit experiment but with two detectors measuring the biphoton amplitude. Each of the two quantum states ( $|\psi_{1,2}\rangle$ ) is split by polarization using a PBS (see panel (a)), directing the signal and idler to detectors  $D_1$  and  $D_2$ , respectively, for individual detection.  $D_1$ , which detects the signal photons from both quantum states, has a fixed position. The position is chosen so that  $l'_2 - l'_1 = 2m\pi/\lambda$  for  $m \in \mathbb{N}$ .  $D_2$ , which detects the idler, moves along the  $x$ -axis, and several measurements are taken. In each measurement, the phase between the idler photons changes according to the path difference  $l_2(x) - l_1(x)$ . (c) Phase-matching functions (PMFs): top,  $HG_1$ ; bottom, two Gaussians. These PMFs correspond to the crystal patterns shown in panel (a).

and idler photons to detectors  $D_1$  and  $D_2$ .  $D_1$ , fixed in position, detects signal photons.  $D_2$  detects the idler photons and moves along the  $x$ -axis, altering the phase between idler photons generated from each crystal based on the path difference  $l_2(x_i) - l_1(x_i)$ , where  $l_1(x_i)$  and  $l_2(x_i)$  are the path lengths for the idler photons generated in the first and second crystal, respectively. Here,  $x_i$  is the generalized coordinate of the stage, corresponding to the transverse movement relative to the incident beam.

For a general case of  $|\psi_{1,2}\rangle$ , the overall state is a superposition of both JSAs, incorporating a relative phase between them. This can be expressed as

$$|\psi\rangle = \frac{1}{\sqrt{2}} (|\psi_1\rangle + e^{i\Delta\phi(x_s, x_i)} |\psi_2\rangle). \quad (6)$$

Here,  $\Delta\phi(x_s, x_i) \equiv \Delta\phi$  represents the relative phase resulting from the position of the stages that couple light into the fibers (designated by kinematic states (KS) in Fig. 2(a)), thereby altering the relative path length difference between the signal (idler) photons, generated from different NLPCs. It can be seen that adjusting  $\Delta\phi$  can change the measured output JSI and provide insights into the initial relative phases of the designed JSAs. The phase between the signal photons generated in different crystals is fixed, so the relative phase ( $\Delta\phi$ , Eq. (6)) between the quantum states  $|\psi_{1,2}\rangle$  is determined solely by the phase between the idler photons.

We can express the measured JSI for a given relative phase as the absolute square of the sum of the JSAs with the

relative phase between them. By considering the interference between two JSAs, with relative phases  $\Delta\phi = \alpha, \alpha + \pi$  (where  $\alpha$  is a general phase), the measured JSI can be formulated as follows:

$$\begin{aligned} \text{JSI}_{\text{int}}(\Delta\phi = \alpha) &= |\text{JSA}_1 + e^{i\alpha} \text{JSA}_2|^2 \\ &= \text{JSI}_1 + \text{JSI}_2 + 2 \cos(\alpha) \cdot \text{JSA}_1 \cdot \text{JSA}_2, \\ \text{JSI}_{\text{int}}(\Delta\phi = \alpha + \pi) &= |\text{JSA}_1 + e^{i(\alpha+\pi)} \text{JSA}_2|^2 \\ &= \text{JSI}_1 + \text{JSI}_2 - 2 \cos(\alpha) \cdot \text{JSA}_1 \cdot \text{JSA}_2. \end{aligned} \quad (7)$$

These equations represent matrices, and each element in these matrices can be treated individually. By performing element-wise operations, we can subtract or multiply corresponding elements from one matrix with those of another. This approach allows us to compute the difference between the measured JSIs for different phases, leading to

$$\text{JSI}_{\text{int}}(\Delta\phi = \alpha) - \text{JSI}_{\text{int}}(\Delta\phi = \alpha + \pi) = 4 \cos(\alpha) \cdot \text{JSA}_1 \cdot \text{JSA}_2. \quad (8)$$

We observe that the difference between JSIs for phases  $\alpha$  and  $\alpha + \pi$  is directly proportional to the product of the JSAs of the two NLPCs. The cosine function modulates this proportionality. Our method can be used for any phase  $\alpha$  that gives  $\cos(\alpha) \neq 0$ . However, when  $\cos(\alpha) = 0$ , the JSI difference becomes zero, meaning we cannot reconstruct  $\text{JSA}_2$  based on this metric alone. In such cases, we can simply change our initial phase,  $\alpha$ , by moving the KS.

We assume  $\alpha = 0$ , which simplifies the equation, and we consider  $JSA_1$  as a known reference, allowing us to reconstruct  $JSA_2$  based on the observed JSI difference directly. However, this reconstruction has a limitation: since we need to divide by  $JSA_1$ , it relies on the assumption that  $JSA_1$  is non-zero. To prove our method, we selected reference crystals having a similar JSI to the JSI of the unknown crystal. In this case, the above limitation of having non-zero values is not a problem. However, any reference crystal with a known JSA and with non-zero values in the spectral region of interest can be used to fully reconstruct the unknown crystal's JSA.

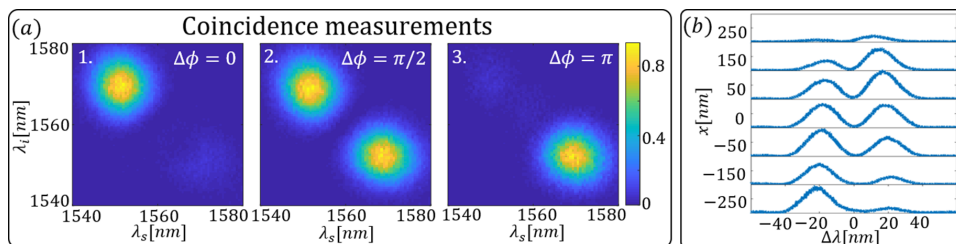
### 3. RESULTS

#### 3.1. Double-Lobe Engineered NLPCs

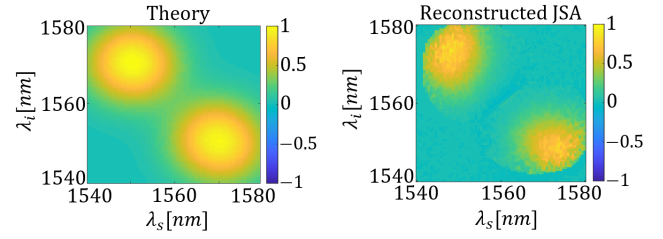
We analyze a case in which the JSA of one of the two crystals corresponds to  $HG_1$ , exhibiting two lobes with opposite phases (Fig. 2(c), top) as a reference, and we used in parallel another crystal in which the JSA is composed of two shifted Gaussian functions that are in phase with each other (Fig. 2(c), bottom). These two different quantum JSAs are produced by employing two distinct engineered NLPCs via electric field poling on a KTP. The crystals were designed by us and fabricated by Raicol Crystals based on our specifications. The design is based on a variation of the duty cycle of the nonlinear modulation [23]. The length of the NLPC was 4 mm and the poling period was 46  $\mu\text{m}$ . When the pump pulse traverses both engineered NLPCs simultaneously (as depicted in Fig. 2(a)), it results in a superposition of two distinct output states that would have been individually obtained from each of the NLPCs. Specifically,  $|\psi_{1,2}\rangle = \frac{1}{\sqrt{2}} (|\omega_{1_s}, \omega_{2_i}\rangle \mp |\omega_{2_s}, \omega_{1_i}\rangle)$  for each design. The overall state is

$$\begin{aligned} |\psi\rangle &= \frac{1}{\sqrt{2}} (|\psi_1\rangle + e^{i\Delta\phi} |\psi_2\rangle) \\ &= \frac{1}{2} ((1 + e^{i\Delta\phi}) |\omega_{1_s}, \omega_{2_i}\rangle + (1 - e^{i\Delta\phi}) |\omega_{2_s}, \omega_{1_i}\rangle). \end{aligned} \quad (9)$$

We generated the entangled photon pair and measured the JSI for different positions of one of the kinematic stages. The measured JSI for three different positions of the stage ( $KS_2$ ) is shown in Fig. 3. The three positions of the stage correspond to three different phase differences  $\Delta\phi = 0, \pi/2, \pi$  (Fig. 3(a)). Changing the relative phase to  $\Delta\phi = 0, \pi$  will result in only one of the lobes (Fig. 3(a)1,3). In the case of a relative phase of  $\Delta\phi = \pi/2$ , the intensity of the two lobes will be equal (Fig. 3(a)2). Figure 3(b) shows the anti-diagonal cross-section of the JSI measured at various positions of the stage ( $KS_2$ ). These results demonstrate an easy transition between different JSIs, which can be useful for quantum information applications.



**Fig. 3.** Interference between NLPCs with two lobes. (a) Measured JSIs for different positions of  $KS_2$ . (b) Measurements of the wavelength difference between the signal and idler for different positions of  $KS_2$ .



**Fig. 4.** Comparison between the theoretical and the reconstructed JSA of the two-lobes NLPC design (see Table 1, second line). The left panel shows the theoretically predicted JSA, while the right panel presents the reconstructed JSA obtained from experimental data. The overlapping integral between the reconstructed and the theoretical JSA is 0.90, demonstrating a high degree of similarity between the experimental results and theoretical predictions.

By using Eqs. (7) and (8), and incorporating the measurements shown in Fig. 3, we reconstructed the JSA of the double-lobe, in-phase NLPC (see Fig. 4). This reconstruction process involves applying the measured JSIs, using the phase information obtained from the experimental setup, and assuming the reference JSA is known. The resulting JSA accurately represents the spectral correlations between photon pairs generated in the SPDC process. The overlap integral between theory and experiment is 0.90, confirming the crystal's expected double-lobe structure and in-phase behavior.

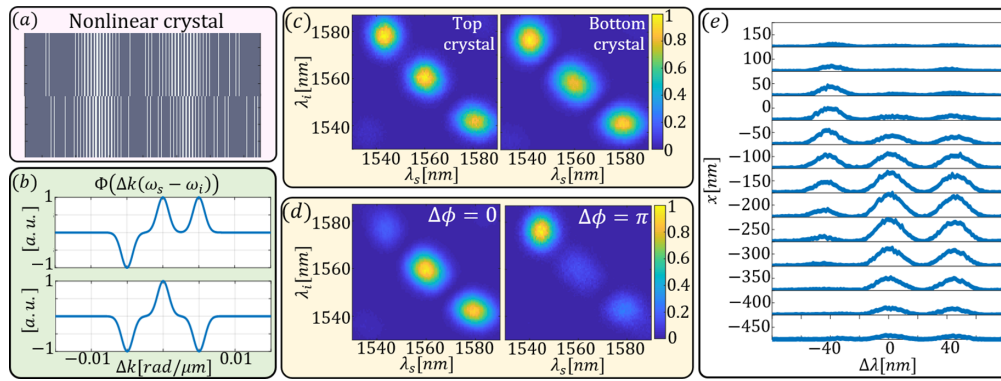
#### 3.2. Three-Lobe Engineered NLPCs

Additionally, we explore another scenario employing the same concept but with different NLPCs. Here, the two engineered NLPCs exhibit a three-lobe shape, as illustrated in Fig. 5(a), with their corresponding PMFs and measured JSI depicted in Figs. 5(b) and 5(c), respectively. The overlapping integrals between the experimental results (Fig. 5(c)) and the theoretical JSIs are 0.97 and 0.95 for the top and bottom crystals, respectively. Specifically for each of the designs, the output state can be written as

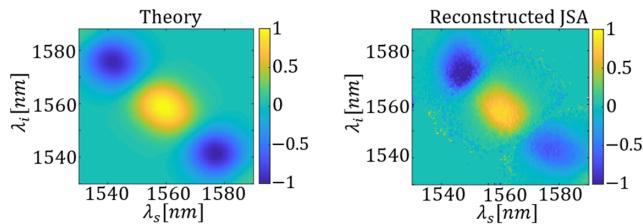
$$|\psi_{1,2}\rangle^{3\text{-lobes}} = \frac{1}{\sqrt{3}} (\mp |\omega_{1_s}, \omega_{3_i}\rangle + |\omega_{2_s}, \omega_{2_i}\rangle - |\omega_{3_s}, \omega_{1_i}\rangle), \quad (10)$$

and the overall state is

$$\begin{aligned} |\psi\rangle^{3\text{-lobes}} &= \frac{1}{\sqrt{2}} (|\psi_1\rangle^{3\text{-lobes}} + e^{i\Delta\phi} |\psi_2\rangle^{3\text{-lobes}}) \\ &= \frac{1}{\sqrt{6}} ((e^{i\Delta\phi} - 1) |\omega_{1_s}, \omega_{3_i}\rangle + (1 + e^{i\Delta\phi}) |\omega_{2_s}, \omega_{2_i}\rangle \\ &\quad - (1 + e^{i\Delta\phi}) |\omega_{3_s}, \omega_{1_i}\rangle). \end{aligned} \quad (11)$$



**Fig. 5.** Interference between crystals having three lobes. (a) The poling pattern of the NLPCs. (b) The phase-matching functions for the upper and lower crystals. (c) JSI measurements of each engineered NLPC operating individually. (d) The JSI measurement of the spectrum resulting from pumping the two NLPCs, for two different positions of the stage ( $KS_2$ ), with corresponding relative phase of 0 and  $\pi$ . Additionally, panel (e) showcases measurements of the marginal spectral distribution as a function of the wavelength difference between the signal and idler for different positions of  $KS_2$ .



**Fig. 6.** Comparison between the theoretical and the reconstructed JSA of the three-lobes NLPC design (see Table 1, bottom line). The left panel shows the theoretically predicted JSA, while the right panel presents the reconstructed JSA obtained from experimental data. The overlapping integral between the reconstructed and the theoretical JSA is 0.86.

We produced an entangled photon pair and examined the JSI for different configurations of one of the coupling stages. The JSI measurements for two distinct positions of the stage ( $KS_2$ ) are illustrated in Fig. 5(d). These positions correspond to two distinct phase differences,  $\Delta\phi = 0, \pi$ . Adjusting the relative phase to  $\Delta\phi = \pi$  results in two lobes nearly disappearing. Conversely, in the absence of a relative phase ( $\Delta\phi = 0$ ), the JSI takes on a complementary form, featuring prominent two lobes and the near absence of the other lobe. In Fig. 5(e), the wavelength difference between the signal and idler, representing their temporal delay, is depicted. This measurement was conducted at various positions of the stage ( $KS_2$ ).

By employing Eqs. (7) and (8) and using the data presented in Fig. 5(d), we obtained the JSA for the three-lobe configuration NLPC (see Fig. 6). This reconstruction uses the measured JSIs and assumes the reference JSA is known. The reconstructed JSA reveals the spectral correlations between the photon pairs produced by the SPDC process, aligning with the crystal’s anticipated three-lobe structure and phase properties. The overlap integral between theory and experiment is 0.86.

#### 4. CONCLUSIONS AND DISCUSSION

In this paper, we introduce an interferometric measurement method using engineered NLPCs to facilitate crystal-based interferometry. This approach enables the reconstruction of the JSA, as demonstrated in our experiments for two NLPCs. This method addresses the limitations of JSI in conventional coincidence

measurements, particularly the absence of phase information. Our findings demonstrate the feasibility of extracting phase information from crystal-based interferometry.

The implications of our work extend beyond immediate advancements in JSI analysis. By interfering biphoton JSAs, this methodology opens doors to more nuanced investigations into quantum phenomena and facilitates the development of novel quantum technologies.

Future research can further enhance this method by addressing factors such as scalability and efficiency to bolster its practical applicability. Additionally, exploring alternative crystal configurations and refining experimental techniques could further enhance the performance and versatility of our methodology. Specifically, one can achieve a more thorough phase analysis by designing an NLPC with a wide rectangular PMF shape and implementing it in our setup as the reference arm. The proposed design overcomes the limitation of JSA reconstruction confined to areas with non-zero reference JSA. We can significantly broaden the range of JSA reconstruction using a wide reference JSA. This setup allows us to extract the JSA of the sample arm effectively. Consequently, our method can be used for straightforward JSA measurement.

Traditionally, obtaining phase information between probability amplitudes of different frequencies requires interference between these amplitudes, typically involving complex and inefficient nonlinear processes. However, our method allows us to gain phase information without resorting to such nonlinear processes, simplifying the procedure significantly. Furthermore, employing our interferometry method is simpler than constructing a standard interferometer, thus offering a more accessible approach to quantum state analysis. This potential application opens new avenues for manipulating and analyzing quantum states more efficiently.

In addition, this method can give many different JSIs (for example, left lobe, two lobes, and right lobe, as shown in Fig. 3(a)) with a small movement of a stage. While our method provides control over the JSI at the measurement stage, it is important to note that the generation process itself remains fixed. This could be useful for applications that require a transition between quantum states of light. Those transitions between different JSIs can also be regarded as rotations in a two-qubit Hilbert space defined by the lobes’ center frequencies for each of

the two photons. These avenues of investigation hold promise for continued advancements in quantum state analysis and quantum information processing.

Our proposed method, based on crystal-based interferometry, shares similarities with traditional phase-shifting interferometry techniques [30], used to reconstruct the phase front of light beams that pass through optical elements. This suggests that our formulation can be extended to incorporate known phase-shifting interferometry methods, potentially offering additional insights and applications. By exploring these connections, we can leverage the strengths of both approaches to enhance the capabilities of quantum state characterization.

**Funding.** Israel Science Foundation (3117/23, 969/22).

**Acknowledgments.** We thank Ziv Gefen from Raicol Crystals for his assistance in preparing the nonlinear crystals. I.H. acknowledges the support of the Weinstein Research Institute for Signal Processing and the Israeli Planning and Budgeting Committee for quantum science and technology research.

**Disclosures.** The authors declare no conflicts of interest.

**Data availability.** Data underlying the results presented in this paper are not publicly available at this time but may be obtained from the authors upon reasonable request.

## REFERENCES

1. F. Flamini, N. Spagnolo, and F. Sciarrino, "Photonic quantum information processing: a review," *Rep. Prog. Phys.* **82**, 016001 (2019).
2. J. L. O'Brien, A. Furusawa, and J. Vučković, "Photonic quantum technologies," *Nat. Photonics* **3**, 687–695 (2009).
3. M. D. Eisaman, J. Fan, A. Migdall, *et al.*, "Invited review article: Single-photon sources and detectors," *Rev. Sci. Instrum.* **82**, 071101 (2011).
4. A. Migdall, S. V. Polyakov, J. Fan, *et al.*, *Single-Photon Generation and Detection: Physics and Applications* (Academic Press, 2013).
5. C. Couteau, "Spontaneous parametric down-conversion," *Contemp. Phys.* **59**, 291–304 (2018).
6. H.-S. Zhong, H. Wang, Y.-H. Deng, *et al.*, "Quantum computational advantage using photons," *Science* **370**, 1460–1463 (2020).
7. J. M. Lukens and P. Lougovski, "Frequency-encoded photonic qubits for scalable quantum information processing," *Optica* **4**, 8–16 (2017).
8. H.-H. Lu, J. M. Lukens, N. A. Peters, *et al.*, "Quantum interference and correlation control of frequency-bin qubits," *Optica* **5**, 1455–1460 (2018).
9. M. Cabrejo-Ponce, A. L. M. Muniz, M. Huber, *et al.*, "High-dimensional entanglement for quantum communication in the frequency domain," *Laser Photonics Rev.* **17**, 2201010 (2023).
10. H.-H. Lu, M. Liscidini, A. L. Gaeta, *et al.*, "Frequency-bin photonic quantum information," *Optica* **10**, 1655–1671 (2023).
11. Y. Shaked, Y. Michael, R. Z. Vered, *et al.*, "Lifting the bandwidth limit of optical homodyne measurement with broadband parametric amplification," *Nat. Commun.* **9**, 609 (2018).
12. N. J. Cerf, M. Bourennane, A. Karlsson, *et al.*, "Security of quantum key distribution using  $d$ -level systems," *Phys. Rev. Lett.* **88**, 127902 (2002).
13. D. Bruß and C. Macchiavello, "Optimal eavesdropping in cryptography with three-dimensional quantum states," *Phys. Rev. Lett.* **88**, 127901 (2002).
14. A. Dosseva, L. Cincio, and A. M. Brańczyk, "Shaping the joint spectrum of down-converted photons through optimized custom poling," *Phys. Rev. A* **93**, 013801 (2016).
15. C. L. Morrison, F. Graffitti, P. Barrow, *et al.*, "Frequency-bin entanglement from domain-engineered down-conversion," *APL Photonics* **7**, 066102 (2022).
16. I. Hurvitz, A. Karnieli, and A. Arie, "Frequency-domain engineering of bright squeezed vacuum for continuous-variable quantum information," *Opt. Express* **31**, 20387–20397 (2023).
17. F. Graffitti, P. Barrow, M. Proietti, *et al.*, "Independent high-purity photons created in domain-engineered crystals," *Optica* **5**, 514–517 (2018).
18. A. Shukhin, I. Hurvitz, S. Trajtenberg-Mills, *et al.*, "Two-dimensional control of a biphoton joint spectrum," *Opt. Express* **32**, 10158–10174 (2024).
19. I. A. Walmsley and C. Dorrer, "Characterization of ultrashort electromagnetic pulses," *Adv. Opt. Photonics* **1**, 308–437 (2009).
20. G. S. Thekkadath, B. A. Bell, R. B. Patel, *et al.*, "Measuring the joint spectral mode of photon pairs using intensity interferometry," *Phys. Rev. Lett.* **128**, 023601 (2022).
21. R.-B. Jin, R. Shiina, and R. Shimizu, "Quantum manipulation of biphoton spectral distributions in a 2d frequency space toward arbitrary shaping of a biphoton wave packet," *Opt. Express* **26**, 21153–21158 (2018).
22. N. Dehghan, A. D'Errico, F. D. Colandrea, *et al.*, "Biphoton state reconstruction via phase retrieval methods," *Optica* **11**, 1115–1123 (2024).
23. R. Shiloh and A. Arie, "Spectral and temporal holograms with nonlinear optics," *Opt. Lett.* **37**, 3591–3593 (2012).
24. A. Leshem, R. Shiloh, and A. Arie, "Experimental realization of spectral shaping using nonlinear optical holograms," *Opt. Lett.* **39**, 5370–5373 (2014).
25. M. Pelton, P. Marsden, D. Ljunggren, *et al.*, "Bright, single-spatial-mode source of frequency non-degenerate, polarization-entangled photon pairs using periodically poled KTP," *Opt. Express* **12**, 3573 (2004).
26. B. S. Shi and A. Tomita, "Generation of a pulsed polarization entangled-photon pair via a two-crystal geometry," *Phys. Rev. A* **67**, 043804 (2003).
27. D. Ljunggren, M. Tengner, P. Marsden, *et al.*, "Theory and experiment of entanglement in a quasi-phase-matched two-crystal source," *Phys. Rev. A* **73**, 032326 (2006).
28. X. Q. Yu, P. Xu, Z. D. Xie, *et al.*, "Transforming spatial entanglement using a domain-engineering technique," *Phys. Rev. Lett.* **101**, 233601 (2008).
29. K. Zielnicki, K. Garay-Palmett, D. Cruz-Delgado, *et al.*, "Joint spectral characterization of photon-pair sources," *J. Mod. Opt.* **65**, 1141–1160 (2018).
30. P. Hariharan, B. F. Oreb, and T. Eiju, "Digital phase-shifting interferometry: a simple error-compensating phase calculation algorithm," *Appl. Opt.* **26**, 2504–2506 (1987).